Solid State Communications 296 (2019) 12–16

Contents lists available at ScienceDirect

Solid State Communications

journal homepage: www.elsevier.com/locate/ssc

Communication

Coulomb blockade correlations in a coupled single-electron device system

Limin Cao[a,*], Fabio Altomare[b,c], Hongli Guo[a], Min Feng[a], Albert M. Chang[b,**]

[a] School of Physics and Technology, Center for Nanoscience and Nanotechnology, and Key Laboratory of Artificial Micro- and Nano-structures of Ministry of Education, Wuhan University, Wuhan, 430072, China
[b] Department of Physics, Duke University, Durham, NC 27708, USA
[c] D-Wave Systems Inc., 3033 Beta Avenue, Burnaby, British Columbia, V5G 4M9, Canada

ARTICLE INFO

Communicated by F. Peeters

Keywords:
Single-electron transistor
Quantum dot
Coulomb blockade
Quantum tunneling

ABSTRACT

Single-electron devices, such as metal single-electron transistor (SET) and semiconductor quantum dot (QD), are Coulomb blockade (CB) devices with promising applications in both quantum and classical beyond-Si information technologies. As an example, a coupled SET-QD system can provide an experimental platform for addressing, manipulating, and detecting spin and/or charge-based qubits for quantum information processing. We have designed and fabricated a prototype device in this family: a series-coupled double quantum dot (DQD) with side-coupled and/or top-coupled Al single-electron transistors (Al-SET), and implemented the readout of the single electron charging and CB behaviors in a QD using the Al-SET. The readout operation is manifested by the correlated CB oscillations taking place separately in the SET and in the QD; these oscillations originate from that the change of electrons one by one in the QD. We have developed an electrostatics model to study the CB correlations in the capacitively coupled QD/Al-SET device system, which shows qualitative agreement with our experimental observations. Moreover, our design and device fabrication are compatible with modern semiconductor techniques, and can potentially be scaled up into larger integrated systems with quantum and classic bit operation and measurement circuitry.

1. Introduction

As the continuous scaling down of device sizes and scaling up of integration have been pushing conventional semiconductor devices towards reaching their physical limits, there is an urgent need to develop next generation technologies, in terms of both device structure and device physics [1–8]. One such technology is the single-electron device platform, which includes the metal single-electron transistor (SET) and the semiconductor quantum dot (QD), whose operation is based on Coulomb blockade (CB) and single electron tunneling effects [9–19]. The most remarkable property of single-electron devices, that makes them appealing for classical information processing beyond the CMOS scheme, is that the switching between ON and OFF states is produced by the addition or removal of one single electron. This ability makes it ideal for reducing circuit power dissipation [9–19]. However, single electron devices have the intrinsic drawback of formidable sensitivity to both environment and device size variations, which represents a major challenge for their implementation in large scale integration [20]. Nevertheless, the unparalleled sensitivity of single-electron devices offers a unique opportunity to use these devices as a building block in quantum integrated circuits, especially when used for quantum state readout. The seminal work by Schoelkopf and Lu et al. demonstrated that the SETs can approach the quantum limit of charge sensitivity [21,22].

Building a large-scale quantum processor is of tremendous interest in both academia and industry, where practical and theoretical research continue to pursue different qubit candidates, such as trapped ions, superconducting circuits, quantum dots, optical lattices, nitrogen-vacancy centers in diamond, etc. However, for a proposed quantum computer to be practical, and to become functional in general usage by the public, it is advantageous for a solid state quantum processor constructed from integrated qubits to be fabricated using the accepted industry-wide techniques, particularly in applications where the quantum circuitry is in close proximity to a conventional microprocessor. In this respect, the lithographically defined few-electron semiconductor QDs have attracted great attention as potentially viable qubits. While they exhibit short coherence times, they facilitate the realization of a solid-state quantum circuit with integrated qubits for the construction of a scalable quantum machine [23–34]. The first experimental results from a few-electron triple dot realized by Gaudreau et al. showed that the

* Corresponding author.
** Corresponding author.
E-mail addresses: limincao@whu.edu.cn (L. Cao), yingshe@phy.duke.edu (A.M. Chang).

https://doi.org/10.1016/j.ssc.2019.04.004
Received 26 November 2018; Received in revised form 24 March 2019; Accepted 9 April 2019
Available online 15 April 2019
0038-1098/

complex QD systems have promising applications in both quantum information and quantum cellular automata (QCA) architectures [35]. Furthermore, single and coupled QD have allowed to simulate artificial atoms, study novel Kondo physics and other charge/spin-correlated quantum phenomena in a regime inaccessible to other systems [36–42]. For example, a continuous quantum state transition from single-peak to double-peak Kondo resonances resulting from spin entanglement has been uncovered in a parallel-coupled DQD [43]. Using a semiconductor QD array, Hensgens et al. was able to simulate the quantum Fermi-Hubbard model, and further proved that a coupled QD system would enable quantum simulation efforts of more complex many-body systems [44].

One crucial issue for quantum information processing is the ability to read out the quantum states of the qubits with high fidelity but minimal backaction. For this task, the metal SET is particularly suitable as it allows electrometry at the quantum limit [20–22,45,46]. Quantum integrated circuits built with a coupled SET and QD system is therefore one of the promising ways for practical quantum information processing, considering scalability and manufacturability. In a prototype of coupled one-dot-one-SET system, Lu et al. implemented real-time detection of electron tunneling in QD using an Al-SET [22]; Veldhorst et al. demonstrated a gate-addressable QD qubit with high fidelity [29]; Chen et al. and Berman et al. studied the metastable excited states and quantum fluctuations of charge in a closed QD with the probe of Al-SET [47,48]. In this study, we report the design and fabrication of a double QD and double SET (DQD-DSET) coupled device, where a series-coupled DQD might potentially be used as the quantum information carrier and operator [23,24], and SETs could readout the quantum state. Our process of fabricating devices using one-step, shadow evaporation technique is applicable to construct scalable integrated quantum devices with control and measurement circuitry. In our experiments, clear single-electron tunneling CB in the QD has been read-out using an Al-SET, as indicated by the correlated CB oscillations from QD and SET in the coupled system. The CB correlations of the QD and SET are modeled using a standard electrostatics model in terms of the electrostatic energies of the capacitively coupled QD-SET system. The predictions of the electrostatic model are in good agreement with our experimental observations. Our demonstration of the DQD-DSET device architecture shows great versatility for the construction of larger-scale integrated systems because the one-step lithography and metallization process favors the protection of the fragile single-electron devices, especially metal SETs, from the danger of electrostatic shocks. Our research also demonstrated that, to realize the practical QD-SET based quantum machines, a high-quality GaAs/AlGaAs heterostructure is a must. Furthermore, the multi-QD-multi-SET architecture is versatile and could be readily transferred to Si platform for physical implementation of scalable quantum hardware that combines desirable quantum coherence and scaling, and for controllable construction of hybrid systems that blend quantum and classical semiconductor hardware approaches.

2. Experimental

2.1. Device fabrication

The devices were fabricated using a one-step process on a GaAs/AlGaAs heterostructure containing a two-dimensional electron gas (2DEG) 100 nm below the surface. The 2DEG has an electron density of $\sim 2.3 \times 10^{11}\,\mathrm{cm}^{-2}$, and a low-temperature mobility of $\sim 1.0 \times 10^{6}\,\mathrm{cm}^{2}\mathrm{V}^{-1}\mathrm{s}^{-1}$ at 4.2 K. The devices on the wafers were patterned by electron beam lithography in a PMMA/MMA bilayer resist. Thermal evaporation was used after pattern definition to deposit two separate 25 nm thick aluminum layers. The first Al layer was oxidized in 100 mTorr of oxygen for about 10 min to form a thin aluminum oxide layer. Then the second angle evaporation of Al was performed to form the tunnel junctions of the SET by the nanometer scale overlap between the two Al lines. In our devices, the $Al/Al_2O_3/Al$ junction area has a typical size of 60 nm × 60 nm achieved by carefully controlling the evaporation angles.

2.2. Device measurements

The electrical measurements were carried out in a He^3 refrigerator operating at a base temperature of 300 mK. A home-made 8 channel voltage source provided high-stability voltages to energize the gates for the formation of QDs. Two home-made current preamplifiers were used to measure the currents passing through the QD and through the SET. For the SET circuit in the charge detection measurements, a small AC signal (typical 23.3 Hz) generated from a Princeton Applied Research 124 lock-in amplifier (PAR124) was added on top of the DC voltage. The AC signals passing through the SET were detected by the same PAR124 lock-in amplifier. This wiring scheme allowed us to perform synchronous measurements on QD and SET. All the DC signals were measured using HP3478A multimeters and recorded by LabVIEW programs in the computer.

3. Results and discussion

In our device architecture each QD is coupled to an SET. The fabrication of the integrated QD-SET coupled devices is performed using a one-step process, thus making this process scalable. In this work, we present a prototype of DQD-DSET device architecture where the two QDs are coupled in series, and each QD is capacitively parallel-coupled to an SET. Two kinds of device configurations are designed: the lateral configuration in which the QD and SET are capacitively side-coupled, and the vertical configuration where SETs are located on top of the QDs. The merit of these designs is that a single QD-SET device could simultaneously perform quantum manipulation and measurement. Moreover, it could practically be scaled into larger integrated quantum circuits and machines. Here in the main text, we present the experimental data from a side-coupled QD-SET device with lateral configuration. The results from a vertical configuration device are presented in Supplementary material (Fig. S1 and S2).

Fig. 1(a) shows a scanning electron microscopy (SEM) micrograph of our device. Here, a series-coupled DQD can be formed when negative voltages are applied to the metallic gates (terminals 1,3,4,6,8,9,10,11,12) to electrostatically confine two droplets of electrons in the 2DEG. Terminal 10 can control the coupling strength between the two dots. Two single SETs between leads 1 and 3 (left SET) and leads 4 and 6 (right SET) are formed through small $Al/Al_2O_3/Al$ tunnel junctions. The two SETs are capacitively side-coupled to the two dots, respectively. Two indium contacts (connected to terminals 7 and 13 via the 2DEG) form the ohmic electrical contact beneath the heterostructure, which serve as the source and drain leads of the QDs.

We performed the electrical measurements in a He^3 refrigerator at 300 mK. In our device, the gate 12 leaked when the applied negative voltage exceeds −1.2 V. Consequently, the left QD could not be formed. We were able to characterize the right dot by energizing gates 3,4,6,8,9,10, and the right SET coupled to it. Fig. 1(b) and (c) show the CB oscillations of the right dot and the right SET as a function of the bias voltage V_g on the plunger gate 9, respectively. Both the QD and SET clearly show smooth periodically spaced conductance peaks, corresponding to the single electron charging and CB effect as the plunger gate voltage is swept. From the geometry and the electrical measurements, we estimated that the total capacitance (C_d) of the dot is about 2.17×10^{-16} F, and the charging energy (E_{cd}) is about 0.368 meV. The period of the CB peaks is determined by the gate-dot capacitance C_{gd} according to $\Delta V_{gd} = e/C_{gd}$, where $e = 1.602 \times 10^{-19}$ C is the electric charge of an electron. We then experimentally determine the C_{gd} to be about 3.20×10^{-17} F ($\Delta V_{gd} \approx 5.0$ mV). Similarly, we deduce the device parameters of SET from its *I-V* characteristics, total capacitance of SET (C_s) about 8.90×10^{-16} F, total resistance (R) about 193 kΩ, and charging energy $E_{cs} \approx 89.5$ μeV. With the 2DEG grounded, the SET

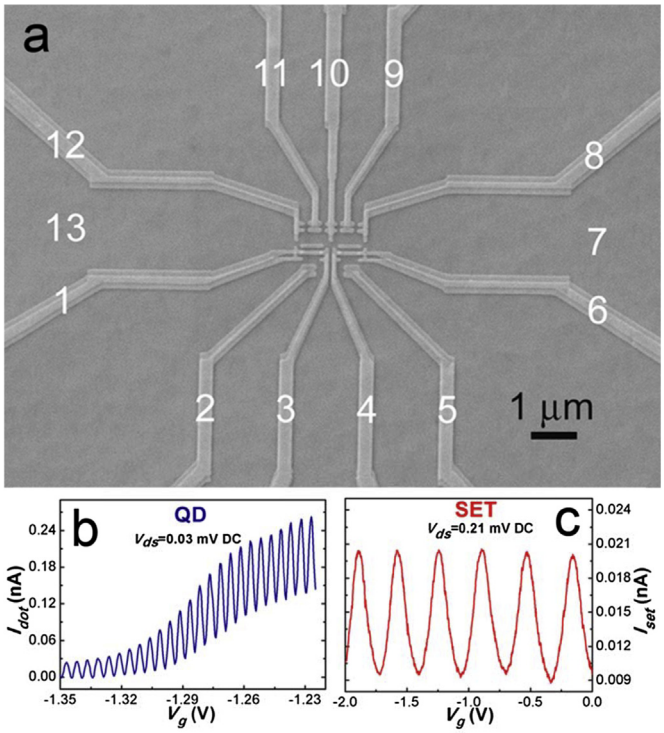

Fig. 1. (a) SEM image of the SET-QD coupled device. Terminals 7 and 13 are connected to the 2DEG by indium ohmic contacts, serving as the source and drain of the QD. (b) Current through the right QD as a function of V_g on gate 9 at low drain-source bias of 0.03 mV (DC), showing CB oscillation. (c) CB oscillation in the right SET at drain-source bias of 0.21 mV (DC) when 2DEG is grounded.

oscillation spacing is about 346.8 mV, giving a nominal gate-SET capacitance (C_{gs}) of 4.62×10^{-19} F.

After confirming that both the QD and SET work properly, we simultaneously activate the right QD and SET by energizing gates 3,4,6,8,9,10 with negative voltages. The DC voltages of the leads 4 and 6 were kept identical. A low-frequency AC voltage (~0.28 mV, 23.3 Hz) is added on top of the DC voltage applied to leads 4 and 6, and this AC voltage is used to bias the right SET. The right QD was held at a small drain-source (leads 7 and 13, 0.03 mV) DC bias. The QD is coupled to drain and source leads through two quantum point contacts, formed in-between leads 3-4-10, and leads 6-8, respectively. We performed the measurements by scanning the bias voltage, V_g, on the QD plunger gate 9. The currents flowing through the QD (I_{dot}) and SET (I_{set}) were recorded simultaneously using two current amplifiers as the gate V_g was sweeping. Fig. 2 displays I_{dot} and I_{set} as a function of V_g. We can clearly

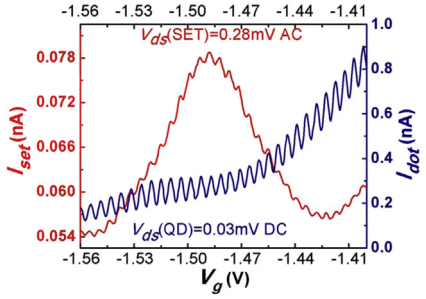

Fig. 2. Current signals from QD and SET versus plunger gate voltage V_g. The current (blue) through QD shows simple, single-period CB oscillation. The SET signal (red) displays a fast-short-period oscillation superimposed on a large-period oscillation. (For interpretation of the references to colour in this figure legend, the reader is referred to the Web version of this article.)

see that, in the curve for I_{set}, a sawtooth-like short-period oscillation with small fluctuation amplitude is superposed on a much longer-period larger-amplitude oscillation. The small amplitude oscillation has the identical period with that from the I_{dot}, the CB oscillation of the QD. The sweeping of V_g causes the electrons in the QD to vary one by one, giving rise to the CB oscillation in I_{dot}. This charge variation in turn causes the induced charges on the SET island to fluctuate in a small fraction of e at the same frequency of QD oscillation. On the other hand, the gate voltage also introduces a slow but linear change in SET charge through the small, direct coupling C_{gs}. The QD induced charge variation oscillates through several full cycles, one for each electron, before the gate voltage induced SET charge changes by one. This is the reason why I_{set} curves show two periodic oscillations, a short-period wave oscillating on top of a large-period one. In the limit of gate-SET capacitance (C_{gs}) much smaller than gate-dot capacitance (C_{gd}), $C_{gs} \ll C_{gd}$, the SET used as an electrometer has only very weak backaction to the QD [49]. The properties of QD thus remain mostly undisturbed. In this case the I_{dot} curves in our measurements feature a single, short-period CB oscillation, similarly to what an independent QD does. However, besides the correlated two-period oscillations from SET, it should be noted that the period of the large-amplitude oscillation in SET changes to about 133 mV when the 2DEG is floated and QD is formed next to it, giving a nominal C_{gs} of about 1.205×10^{-18} F. While, the period of CB oscillation in QD has a typical value of about 5.44 mV (corresponding to a nominal C_{gd} of $\sim 2.95 \times 10^{-17}$ F). The discrepancy of less than 10% most likely comes from the geometry changes of the QD when different negative voltages are applied to the metallic gates. The above experimental observations clearly demonstrate that we have realized the read-out of the charge states by sensing individual electron tunneling events and CB behaviors of QD using an Al-SET in the coupled SET-QD system.

In our device configuration, the SET and QD are coupled in parallel, and share the same central gate (lead 9). So changing the gate voltage V_g will adjust the offset charges on both. We now use a standard electrostatic coupling model, as shown in Fig. 3, to study the coupled QD-SET system where the discrete quantum states are not taken into account [50–52]. With a given charge configuration (N_d in QD, N_s in SET, see Fig. 3), the respective electrostatic energies of QD and SET at zero bias are given by

$$U_{QD} = \frac{\left[V_g C_{gd} - N_d|e| + (V_g C_{gs} - N_s|e|)\frac{C_m}{C_s}\right]^2}{2C_d\left(1 - \frac{C_m^2}{C_s C_d}\right)^2} \quad (1)$$

$$U_{SET} = \frac{\left[V_g C_{gs} - N_s|e| + (V_g C_{gd} - N_d|e|)\frac{C_m}{C_d}\right]^2}{2C_s\left(1 - \frac{C_m^2}{C_s C_d}\right)^2} \quad (2)$$

where $N_{d(s)}$ is the number of uncompensated electrons in QD(SET), C_m is the SET-QD coupling capacitance, $C_{d(s)}$ is the total capacitance of the QD(SET) to the environment including C_m, and $C_{gd(s)}$ is the gate-QD

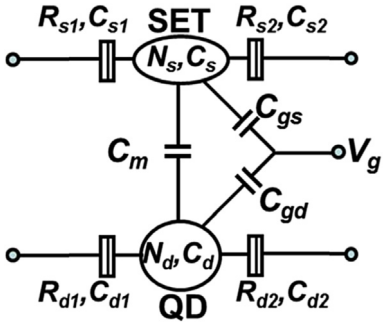

Fig. 3. Model diagram of the QD-SET coupled system.

(SET) capacitance. Then the electrochemical potentials of the QD and SET are given by

$$\mu_d(N_d, N_s) = U_{QD}(N_d, N_s) - U_{QD}(N_d - 1, N_s) = \frac{\left(N_d - \frac{1}{2} + N_s\frac{C_m}{C_s}\right)e^2 - V_g|e|\left(C_{gd} + C_{gs}\frac{C_m}{C_s}\right)}{C_d\left(1 - \frac{C_m^2}{C_sC_d}\right)^2} \quad (3)$$

$$\mu_s(N_s, N_d) = U_{SET}(N_s, N_d) - U_{SET}(N_s - 1, N_d) = \frac{\left(N_s - \frac{1}{2} + N_d\frac{C_m}{C_d}\right)e^2 - V_g|e|\left(C_{gs} + C_{gd}\frac{C_m}{C_d}\right)}{C_s\left(1 - \frac{C_m^2}{C_sC_d}\right)^2} \quad (4)$$

The electrochemical potentials of the QD and SET devices determine their stabilities (whether or not the number of electrons in the devices changes). When the gate voltage V_g changes by ΔV_{g1}, thus changing the charge on QD by one, e.g. N_d to N_d+1, the device will reach the minimum energy states with equal electrochemical potentials at the equilibrium points. So from

$$\mu_d(N_d, N_s; V_g) = \mu_d\left(N_d + 1, N_s + \frac{\Delta V_{g1}C_{gs}}{|e|}; V_g + \Delta V_{g1}\right) \quad (5)$$

we can obtain $\Delta V_{g1} = |e|/C_{gd}$. ΔV_{g1} is the period of QD CB oscillation, corresponding to the addition of a single electron to the QD as a function of V_g. Similarly from

$$\mu_s(N_s, N_d; V_g) = \mu_s\left(N_s + 1, N_d + \frac{\Delta V_{g2}C_{gd}}{|e|}; V_g + \Delta V_{g2}\right) \quad (6)$$

we can obtain $\Delta V_{g2} = |e|/C_{gs}$. This is the larger period of the Coulomb oscillations in SET corresponding to adding one electron to SET island, caused by direct coupling of SET to the gate with a much smaller SET to gate capacitance. When the occupancy of QD changes by one electron, then

$$\mu_s(N_d, N_s; V_g) = \mu_s\left(N_d + 1, N_s + \frac{\Delta V_{g3}C_{gs}}{|e|}; V_g + \Delta V_{g3}\right) \quad (7)$$

We then obtain $\Delta V_{g3} = |e|/C_{gd}$. We see that ΔV_{g3} is equal to ΔV_{g1}. In our experiments, we show that the sawtooth like faster oscillation in I_{set} has the same period as that in QD, indicating that they indeed result from the changes in N_d. The periodic oscillation in I_{dot} and the faster component in I_{set} both originate from the tunneling of electrons in the QD one by one. So the individual tunneling of electrons in QD has been detected by the Al-SET electrometer in our QD-SET coupled system, demonstrating that the Al-SET reads out the quantum states of the QD.

Now we consider the phase relationship of the CB oscillation in QD and the sawtooth like short-period oscillation from SET. From our experimental data and the electrostatic analyses, we know that the periodic CB oscillation in I_{dot} and the faster oscillation peaks in I_{set} on top of the slowly varying background are both induced by the tunneling of electrons in the QD one by one. For a simplification purpose, we only consider the case of zero bias in the linear transport regime. For a CB device, such as the QD and SET, a conductance resonance occurs whenever two neighboring charge states become degenerate, i.e., whenever the electrostatic energy parabolas for N and $N+1$ electrons meet in one point. Then from Equations (1) and (2), we can obtain the energy degeneracy points giving rising to the CB resonance peaks for QD and SET as

$$V_g(QD) = \frac{\left(N_d + \frac{1}{2}\right)|e| + \left(N_s + \frac{C_{gs}}{2C_{gd}}\right)\frac{C_m}{C_s}|e|}{C_{gd} + C_{gs}\frac{C_m}{C_s}} \quad (8)$$

$$V_g(SET) = \frac{\left(N_s + \frac{1}{2}\right)|e| + \left(N_d + \frac{C_{gd}}{2C_{gs}}\right)\frac{C_m}{C_d}|e|}{C_{gs} + C_{gd}\frac{C_m}{C_d}} \quad (9)$$

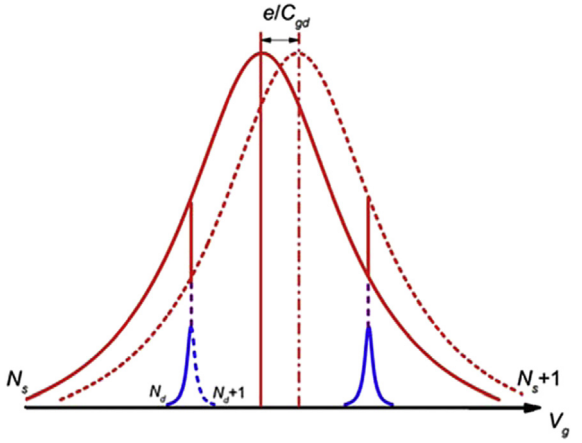

Fig. 4. Schematic diagram of the CB correlations in the coupled SET-QD system. The blue small-amplitude peaks denote the CB resonance peaks induced by the change of electrons in the QD by one. The integer changes of electrons in QD one by one induce a periodic shift of the SET CB resonance peak by $\Delta V_g^m = |e|/C_{gd}$, which gives rise to a sawtooth like oscillation superposed on the large-amplitude CB resonance peak. (For interpretation of the references to colour in this figure legend, the reader is referred to the Web version of this article.)

$V_g(QD)$ and $V_g(SET)$ correspond to the gate bias values where the CB resonance peaks of QD and SET (the large-period oscillation peaks from SET) take place, when the electrons on QD and SET are changed from $N_{d(s)}$ to $N_{d(s)}+1$, respectively. From Equations (8) and (9), we can extract the periods of CB oscillations in QD and SET, $\Delta V_g(QD) = |e|/C_{gd}$ and $\Delta V_g(SET) = |e|/C_{gs}$, which is consistent with the above analyses. Since C_{gs} is much smaller than C_{gd}, this makes the SET CB oscillation period much larger than that of QD. However, when N_d changes by one, which gives rise to one CB resonance peak, the QD-SET internal polarization changes, causing the SET conductance resonance peak to shift by $\Delta V_g^m = |e|/C_{gd}$, as shown in Fig. 4. The integer changes of N_d one by one thus induce a periodic shift of the SET CB resonance peak, which results in a sawtooth like, periodic rising or decreasing of the current passing through the SET. This produces the faster short-period oscillation with periodicity of $|e|/C_{gd}$, which is superposed on the top of a large-period background oscillation in I_{set}. Since adding one electron on QD can only produce a polarized charge on SET with a small fraction of e, thus the fast oscillation is characterized by the small amplitude. The sharp turning points of the sawtooth like oscillation correspond to the CB resonance peaks of QD, since both are introduced by the changes of N_d by one. This suggests that they should be in-phase or have the inverted phase relationship, depending on the charge states and surroundings of the QD and SET. Fig. 2 shows that CB resonance oscillation of QD is nearly in-phase with that of the sawtooth like fast oscillation component in SET. However, in our experiment, the measurements indicate that these two oscillations are often neither fully in-phase nor out of phase, though they have the same frequency. This discrepancy may be caused by the environmental charges, including the movable surface state charges, dangling bonds, the electron fluctuation in 2DEG, etc. All of these external charges will introduce phase shift of the oscillation peaks.

4. Conclusions

In summary, we have fabricated DQD-DSET coupled devices using a one-step lithography and metallization process. The one-step fabrication process is desirable for the construction of scalable integrated circuits built from fragile quantum devices. The DQDs are coupled in series, and might work as the quantum information carrier and processor [23,24]. Two SETs are capacitively parallel-coupled to the two dots, respectively, and are intended to readout the quantum states of

the dots. The single-electron tunneling CB states in QD were clearly read-out using the SET. We developed a simple standard capacitively coupling model to account for the CB correlations in the coupled QD-SET device. The description is in good agreement with our experimental results.

This device architecture integrates the processor with reader in close proximity in the circuit, and can be made using the one-step approach with high fidelity, thus provides increased flexibility in design and fabrication. The device design, materials, and fabrication are compatible with existing semiconductor technologies, offering the prospect of integrating quantum devices with practical functionality and scalability. Furthermore, the similarity of the QD/SET and conventional semiconductor transistor in device architecture, fabrication, and manipulation might offer the opportunity to design and construct hybrid integrated circuits, which takes advantage of both the quantum and conventional devices for information processing. Our results demonstrated that, for the implementation of the practical QD-SET quantum machines, a high quality 2DEG which hosts the quantum devices is a must. Further research might move our multi-QD-multi-SET design and architecture to isotopically purified silicon materials and heterostructures [53], which generally offer long coherence times and promising scaling for quantum hardware [54–57], crucial for practical quantum machines.

Competing financial interests

The authors declare no competing financial interests.

Acknowledgements

We thank F.X. Zhang and C.W. Lin for helpful discussions, and G. Poulin-Lamarre for careful reading of the manuscript. This research was supported in part by National Science Foundation, United States (NSF, project No. DMR-0401648) and Natural Science Foundation of China, China (NSFC, project No. 1157041197).

Appendix A. Supplementary data

Supplementary data to this article can be found online at https://doi.org/10.1016/j.ssc.2019.04.004.

References

[1] K. Ziemelis, Nature 406 (2000) 1021.
[2] P.S. Peercy, Nature 406 (2000) 1023.
[3] I. Osborne, M. Lavine, R. Coontz, Science 327 (2010) 1595.
[4] T.N. Theis, P.M. Solomon, Science 327 (2010) 1600.
[5] L. Venema, Nature 479 (2011) 309.
[6] A.M. Ionescu, H. Riel, Nature 479 (2011) 329.
[7] R. Chau, B. Doyle, S. Datta, J. Kavalieros, K. Zhang, Nat. Mater. 6 (2007) 810.
[8] M.M. Waldrop, Nature 530 (2016) 145.
[9] K.S. Makarenko, Z.H. Liu, M.P. de Jong, F.A. Zwanenburg, J. Husken, W.G. van der Wiel, Adv. Mater. 29 (2017) 1702920.
[10] O. Bitton, D.B. Gutman, R. Berkovits, A. Frydman, Nat. Commun. 8 (2017) 802.
[11] K. Willing, H. Lehmann, M. Volkmann, C. Klinke, Sci. Adv. 3 (2017) e1603191.
[12] V. Ray, R. Subramanian, P. Bhadrachalam, L.C. Ma, C.U. Kim, S.J. Koh, Nat. Nanotechnol. 3 (2008) 603.
[13] K. Likharev, Proc. IEEE 87 (1999) 606.
[14] L.J. Guo, E. Leobandung, S.Y. Chou, Science 275 (1997) 649.
[15] S.J. Shin, C.S. Jung, B.J. Park, T.K. Yoon, J.J. Lee, S.J. Kim, J.B. Choi, Y. Takahashi, D.G. Hasko, Appl. Phys. Lett. 97 (2010) 103101.
[16] M.A. Kaster, Rev. Mod. Phys. 64 (1992) 849.
[17] D.V. Averin, K.K. Likharev, J. Low Temp. Phys. 62 (1986) 345.
[18] T.A. Fulton, G.J. Dolan, Phys. Rev. Lett. 59 (1987) 109.
[19] M. Ciorga, A.S. Sachrajda, P. Hawrylak, C. Gould, P. Zawadzki, S. Jullian, Y. Feng, Z. Wasilewski, Phys. Rev. B 61 (2000) R16315.
[20] M.H. Devoret, R.J. Schoelkopf, Nature 406 (2000) 1039.
[21] R.J. Schoelkopf, P. Wahlgren, A.A. Kozhevnikov, P. Delsing, D.E. Prober, Science 280 (1998) 1238.
[22] W. Lu, Z.Q. Ji, L. Pfeiffer, K.W. West, A.J. Rimberg, Nature 423 (2003) 422.
[23] D. Loss, D.P. DiVincenzo, Phys. Rev. A 57 (1998) 120.
[24] D.P. DiVincenzo, Fortschr. Phys. 48 (2000) 771.
[25] R. Hanson, L.P. Kouwenhoven, J.R. Petta, S. Tarucha, L.M.K. Vandersypen, Rev. Mod. Phys. 79 (2007) 1217.
[26] J.R. Petta, A.C. Johnson, J.M. Taylor, E.A. Laird, A. Yacoby, M.D. Lukin, C.M. Marcus, M.P. Hanson, A.C. Gossard, Science 309 (2005) 2180.
[27] K.C. Nowack, M. Shafiei, M. Laforest, G.E.D.K. Prawiroatmodjo, L.R. Schreiber, C. Reichl, W. Wegscheider, L.M.K. Vandersypen, Science 333 (2011) 1269.
[28] M.D. Shulman, O.E. Dial, S.P. Harvey, H. Bluhm, V. Umansky, A. Yacoby, Science 336 (2012) 202.
[29] M. Veldhorst, J.C.C. Hwang, C.H. Yang, A.W. Leenstra, B. de Ronde, J.P. Dehollain, J.T. Muhonen, F.E. Hudson, K.M. Itoh, A. Morello, A.S. Dzurak, Nat. Nanotechnol. 9 (2014) 981.
[30] B.M. Maune, M.G. Borselli, B. Huang, T.D. Ladd, P.W. Deelman, K.S. Holabird, A.A. Kiselev, I. Alvarado-Rodriguez, R.S. Ross, A.E. Schmitz, M. Sokolich, C.A. Watson, M.F. Gyure, A.T. Hunter, Nature 481 (2012) 344.
[31] D. Kim, Z. Shi, C.B. Simmons, D.R. Ward, J.R. Prance, T.S. Koh, J.K. Gamble, D.E. Savage, M.G. Lagally, M. Friesen, S.N. Coppersmith, M.A. Eriksson, Nature 511 (2014) 70.
[32] J. Medford, J. Beil, J.M. Taylor, E.I. Rashba, H. Lu, A.C. Gossard, C.M. Marcus, Phys. Rev. Lett. 111 (2013) 050501.
[33] B.C. Wang, G. Cao, H. Li, M. Xiao, G.C. Guo, X.D. Hu, H.W. Jiang, G.P. Guo, Phys. Rev. Appl. 8 (2017) 064035.
[34] A.J. Landig, J.V. Koski, P. Scarlino, U.C. Mendes, A. Blais, C. Reichl, W. Wegscheider, A. Wallraff, K. Ensslin, T. Ihn, Nature 560 (2018) 179.
[35] L. Gaudreau, S.A. Studenikin, A.S. Sachrajda, P. Zawadzki, A. Kam, J. Lapointe, M. Korkusinski, P. Hawrylak, Phys. Rev. Lett. 97 (2006) 036807.
[36] L.P. Kouwenhoven, C.M. Marcus, Phys. World 11 (1998) 35.
[37] L.P. Kouwenhoven, L. Glazman, Phys. World 14 (2001) 33.
[38] D. Goldhaber-Gordon, H. Shtrikman, D. Mahalu, D. Abusch-Magder, U. Meirav, M.A. Kaster, Nature 391 (1998) 156.
[39] S.M. Cronenwett, T.H. Oosterkamp, L.P. Kouwenhoven, Science 281 (1998) 540.
[40] Y. Ji, M. Heiblum, D. Sprinzak, D. Mahalu, H. Shtrikman, Science 290 (2000) 779.
[41] H. Jeong, A.M. Chang, M.R. Melloch, Science 293 (2001) 2221.
[42] N.J. Craig, J.M. Taylor, E.A. Lester, C.M. Marcus, M.P. Hanson, A.C. Gossard, Science 304 (2004) 565.
[43] J.C. Chen, A.M. Chang, M.R. Melloch, Phys. Rev. Lett. 92 (2004) 176801.
[44] T. Hensgens, T. Fujita, L. Janssen, X. Li, C.J. Van Diepen, C. Reichl, W. Wegscheider, S. Das Sarma, L.M.K. Vandersypen, Nature 548 (2017) 70.
[45] J.J. Pla, K.Y. Tan, J.P. Dehollain, W.H. Lim, J.J.L. Morton, D.N. Jamieson, A.S. Dzurak, A. Morello, Nature 489 (2012) 541.
[46] J. Bylander, T. Duty, P. Delsing, Nature 434 (2005) 361.
[47] J.C. Chen, A.H. An, T. Ueda, S. Komiyama, K. Hirakawa, V. Antonov, Phys. Rev. B 74 (2006) 045321.
[48] D. Berman, N.B. Zhitenev, R.C. Ashoori, M. Shayegan, Phys. Rev. Lett. 82 (1999) 161.
[49] W. Lu, A.J. Rimberg, K.D. Maranowski, A.C. Gossard, Appl. Phys. Lett. 77 (2000) 2746.
[50] A.M. Chang, J.C. Chen, Rep. Prog. Phys. 72 (2009) 096501.
[51] W.G. van der Wiel, S. De Franceschi, J.M. Elzerman, T. Fujisawa, S. Tarucha, L.P. Kouwenhoven, Rev. Mod. Phys. 75 (2003) 1.
[52] I.M. Ruzin, V. Chandrasekhar, E.I. Levin, L.I. Glazman, Phys. Rev. B 45 (1992) 13469.
[53] F.A. Zwanenburg, A.S. Dzurak, A. Morello, M.Y. Simmons, L.C.L. Hollenberg, G. Klimeck, S. Rogge, S.N. Coppersmith, M.A. Eriksson, Rev. Mod. Phys. 85 (2013) 961.
[54] D.M. Zajac, A.J. Sigillito, M. Russ, F. Borjans, J.M. Taylor, G. Burkard, J.R. Petta, Science 359 (2018) 439.
[55] N. Samkharadze, G. Zeng, N. Kalhor, D. Brousse, A. Sammak, U.C. Mendes, A. Blais, G. Scappucci, L.M.K. Vandersypen, Science 359 (2018) 1123.
[56] T.F. Watson, S.G.J. Philips, E. Kawakami, D.R. Ward, P. Scarlino, M. Veldhorst, D.E. Savage, M.G. Lagally, M. Friesen, S.N. Coppersmith, M.A. Eriksson, L.M.K. Vandersypen, Nature 555 (2018) 633.
[57] X. Mi, M. Benito, S. Putz, D.M. Zajac, J.M. Taylor, G. Burkard, J.R. Petta, Nature 555 (2018) 599.